Journal of Sound and Vibration (2000) **234**(4), 591–610
doi:10.1006/jsvi.1999.2878, available online at http://www.idealibrary.com on IDEAL®

STABILIZATION OF MOTION OF HELICOPTER ROTOR BLADES USING DELAYED FEEDBACK—MODELLING, COMPUTER SIMULATION AND EXPERIMENTAL VERIFICATION

J. M. KRODKIEWSKI

Department of Mechanical and Manufacturing Engineering, The University of Melbourne, Parkville, Vic. 3052, *Australia*

AND

J. S. FARAGHER

Aeronautical & Maritime Research Laboratory, Melbourne, Vic. 3052, *Australia*

(*Received* 27 *April* 1999, *and in final form* 14 *December* 1999)

A new control law for stabilizing the periodic motion of uncertain systems, with particular application to helicopter rotor blades, is presented. The control law uses proportional displacement and velocity feedback with a time delay equal to the period of the motion being stabilized. No knowledge of the dynamics of the system being controlled or the desired trajectory is required. The control law is tested on a two-degree-of-freedom mathematical model that approximates the motion of a helicopter rotor blade in both hover and forward flight. Analysis of the developed perturbations equation shows that a significant improvement in the stability of the motion of the rotor blade is achieved by the appropriate choice of the control parameters. The control law greatly affected the transient states without altering the steady state motion of the uncontrolled system. This feature is particularly important for helicopters because the steady state motion of the rotor blades determines the flight path. The experimental investigation confirms the existence of optimal values of the parameters of the control law, which result in a significant improvement of the stability of the periodic motion of the installation. The experimentally obtained relationship between the optimal control parameters and the period of the motion confirms the results of the analytical investigation of the influence of the control law on the stability margin of uncertain systems.

1. INTRODUCTION

Many machines and devices are designed to perform periodic motion. From an engineering point of view, the stability of this periodic motion is essential since its lack leads to poor performance, damage, or even destruction.

If the parameters of a system and its motion are known it is reasonably easy to improve the stability margin of the system. Unfortunately, in the case of helicopter rotor blade problems, the parameters of the system as well as the parameters of its motion are uncertain. Researchers agree that because of their extreme complexity the problems of helicopter rotor aerodynamics and structural dynamics are not understood sufficiently to allow the prediction of rotor exciting forces with any degree of confidence [1–4]. In such a case, an

0022-460X/00/290591 + 20 $35.00/0

active control law, which can improve the stability of the periodic motion, cannot depend explicitly upon the system parameters. However, as Loewy [1] pointed out, "whatever the aerodynamics are, they are periodic". To stabilize periodic motion in cases where the parameters are uncertain, the following time-delay control law was developed [5, 6]:

$$\Delta y = a(x(t) - x(t-\tau)) + b(\dot{x}(t) - \dot{x}(t-\tau)) \tag{1}$$

where a and b are parameters, $x(t)$ and $\dot{x}(t)$ are the current displacement and velocity of the uncertain system, $x(t-\tau)$ and $\dot{x}(t-\tau)$ are the displacement and velocity which the system had one period earlier and Δy is the control input.

By testing the control law (1) on a mathematical model of a one-degree-of-freedom (d.o.f.) non-linear object, Krodkiewski and Faragher [5] concluded that if the time delay τ is equal to the period of the steady state motion of the uncontrolled object, the region of asymptotic stability of its periodic motion is greatly enlarged and the vibration during the transient states is greatly attenuated.

A major feature of the control law (1) is that it does not change the periodic steady state trajectory of the uncontrolled object but greatly influences the transient states of the system. Pyragas [7] developed a similar time-delay control law for stabilizing unstable periodic trajectories in chaotic systems. The most significant difference between the two control laws is that the second term in the control law (1) is not present in the control law developed by Pyragas [7]. The second term introduced in equation (1) plays a very significant role in improving the stability of the steady state motion of the system.

Research studies on active control of the motion of helicopter rotor blades can be divided into two categories. Authors of works which fall into the first category, called higher harmonic control (HHC), assume that the feedback signals come from sensors attached to the helicopter fuselage and that the control inputs are imposed on the conventional swashplate (labelled 1 in Figure 1) by means of actuators (labelled 3 in Figure 1) in the non-rotating system [8, 9].

This gives only three independent control inputs because the swashplate has only three d.o.f. In the other approach, called individual blade control (IBC), sensors are attached to the rotor blades and the control inputs are applied to actuators (labelled 2 in Figure 1) which replace the pitch links that control the rotor blade angle of attack in the rotating system [10, 11]. Recently, other methods for controlling individual rotor blades, such as piezoelectric actuators on the blade [12] or an actively controlled flap [13], have also been investigated. In these methods, the number of the control inputs is equal to the number of blades. The control law (1) can be used with both of the above methods of implementation. To assess the effectiveness of the control law, it was applied to a mathematical model of a helicopter rotor blade.

This paper presents the results of the stability analysis of the steady-state flap and pitch motion of the helicopter rotor blade. The case of hovering flight and the case of forward flight are both considered, in that order. Also, the results of an experimental investigation of the influence of the control law (1) on the stability margin of the periodic motion of a laboratory installation are shown.

2. MATHEMATICAL MODEL OF THE UNCONTROLLED SYSTEM

To test the control law (1), the following mathematical model of the uncontrolled system developed by Stammers [14] was adopted. The mathematical model was based on the physical model shown in Figure 2.

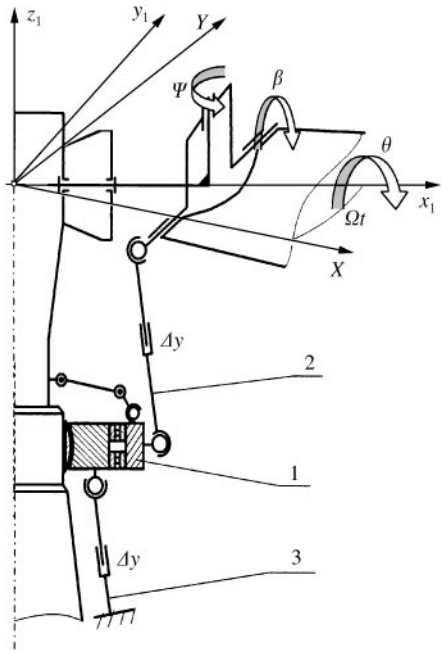

Figure 1. Rotor control linkages.

$$\mathbf{M}(\psi)\ddot{\mathbf{x}} + \mathbf{C}(\psi)\dot{\mathbf{x}} + \mathbf{K}(\psi)\mathbf{x} = [3776v_1^2\, y, 0]^{\mathrm{T}}, \tag{2}$$

where

$$\ddot{\mathbf{x}} = \left[\frac{\mathrm{d}^2\theta}{\mathrm{d}\psi^2}, \frac{\mathrm{d}^2\beta}{\mathrm{d}\psi^2}\right]^{\mathrm{T}}, \quad \dot{\mathbf{x}} = \left[\frac{\mathrm{d}\theta}{\mathrm{d}\psi}, \frac{\mathrm{d}\beta}{\mathrm{d}\psi}\right]^{\mathrm{T}}, \quad \mathbf{x} = [\theta, \beta]^{\mathrm{T}}; \psi = \Omega t, \tag{3}$$

$$\mathbf{M}(\psi) = \begin{bmatrix} 1 & 283\sigma \\ 0 & 1 \end{bmatrix}, \quad \mathbf{C}(\psi) = \begin{bmatrix} 2{\cdot}084(1 + \frac{4}{3}\mu\sin\psi) & 0 \\ 0 & 0{\cdot}8335(1 + \frac{4}{3}\mu\sin\psi) \end{bmatrix},$$

$$\mathbf{K}(\psi) = \begin{bmatrix} v_1^2 & 283\sigma \\ 0{\cdot}8335(0{\cdot}8 + 2\mu\sin\psi + \frac{2}{3}\mu^2(1 - \cos 2\psi)) & (1 + 1{\cdot}111\mu\cos\psi + 0{\cdot}8335\mu^2\sin 2\psi) \end{bmatrix}. \tag{4}$$

The flap and pitch angles are denoted by β and θ respectively. The angular speed of the rotor shaft is denoted by Ω. The pitch natural frequency is denoted by $v_1\Omega$. Therefore v_1 may be considered as the non-dimensional pitch natural frequency. $\psi = \Omega t$ stands for the non-dimensional time, which is the angle of rotation of the rotor shaft about the Z-axis and is called the "azimuth angle". The distance of the centre of gravity behind the aerodynamic centre of the rotor blade expressed as a fraction of the chord dimension c_h is called the "centre of gravity offset" and it is denoted by σ (see Figure 3).

A dot over a variable indicates differentiation with respect to non-dimensional time ψ. The tip-speed ratio μ is the ratio of the velocity of the helicopter relative to the surrounding air, to the velocity of the tip of the rotor blade relative to the helicopter (ΩR_s) (see Figure 2). Since the rotor speed Ω of a helicopter varies only slightly, the tip-speed ratio μ is indicative of the forward speed of the helicopter. In hovering flight $\mu = 0$. The maximum forward flight

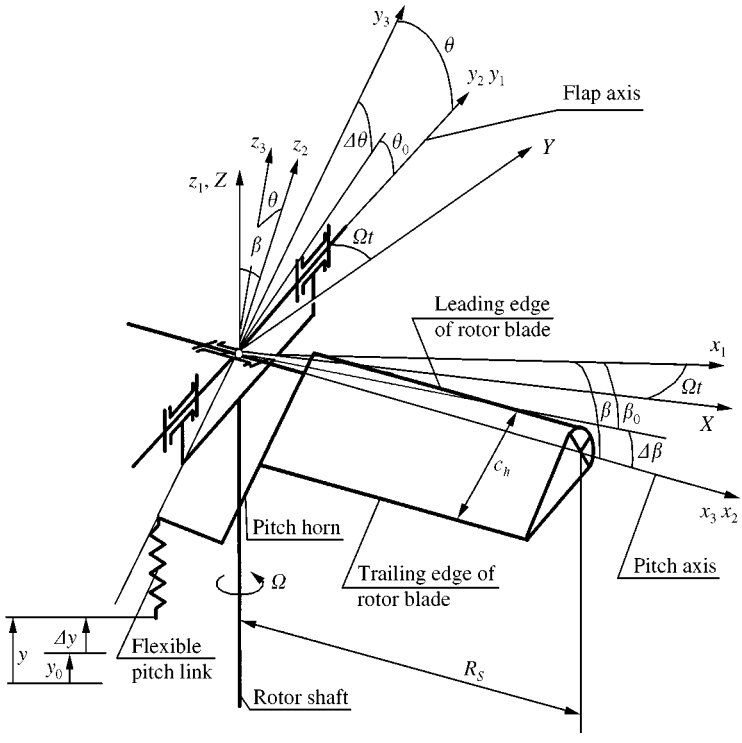

Figure 2. The two-degree-of-freedom physical model of the rotor blade.

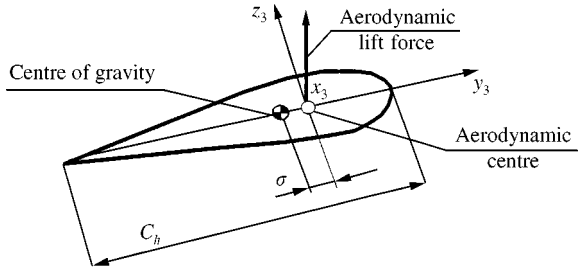

Figure 3. The centre of gravity offset.

speed of helicopters is generally limited to $\mu = 0{\cdot}5$, therefore for the numerical analysis presented in this paper a value of $\mu = 0{\cdot}3$ was used. The displacement of the lower end of the flexible pitch link is denoted by y,

$$y = y_0 + \Delta y. \tag{5}$$

The displacement y_0 is dictated by the pilot and determines the steady state motion of the uncontrolled system. The displacement Δy is the active control input.

The values of the parameters used in the mathematical model were chosen to represent realistic values for a Sikorsky Black Hawk helicopter. The two parameters σ and v_1 in the matrices (4) that affect the pitch-flap stability were chosen as the design parameters.

For a motionless swashplate the displacement y_0 is a periodic function of time,

$$y_0(\psi) = y_0(\psi + 2\pi) \tag{6}$$

and the above mathematical model (2) has a periodic solution

$$\theta_0(\psi) = \theta_0(\psi + 2\pi), \qquad \beta_0(\psi) = \beta_0(\psi + 2\pi). \tag{7}$$

To improve the stability of the periodic motion (7) and control law (1) was adopted. The equations of motion for the helicopter rotor blade with active control are described in the following section.

3. CONTROL LAW

The schematic diagram of the controlled system is shown in Figure 4.
The control input Δy is

$$\Delta y = 0{\cdot}0001a(\beta(\psi) - \beta(\psi - \tau)) + 0{\cdot}0001b(\dot{\beta}(\psi) - \dot{\beta}(\psi - \tau)), \tag{8}$$

where a and b are adjustable control parameters, $\beta(\psi)$ is the flap angle and $\beta(\psi - \tau)$ is the flap angle recorded one period earlier. A factor of 0·0001 was introduced solely for convenience. The time delay in the feedback loop was set equal to the period of one revolution of the helicopter rotor $\tau = 2\pi$. Introduction of equations (5) and (8) into equation (2) yields the equation of motion of the controlled system

$$\mathbf{M}(\psi)\cdot\ddot{\mathbf{x}} + \mathbf{C}(\psi)\cdot\dot{\mathbf{x}} + \mathbf{K}(\psi)\cdot\mathbf{x} = [3776v_1^2\, y_0(\psi), 0]^{\mathrm{T}} + \mathbf{A}(\mathbf{x}(\psi) - \mathbf{x}(\psi - \tau)) + \mathbf{B}(\dot{\mathbf{x}}(\psi) - \dot{\mathbf{x}}(\psi - \tau)), \tag{9}$$

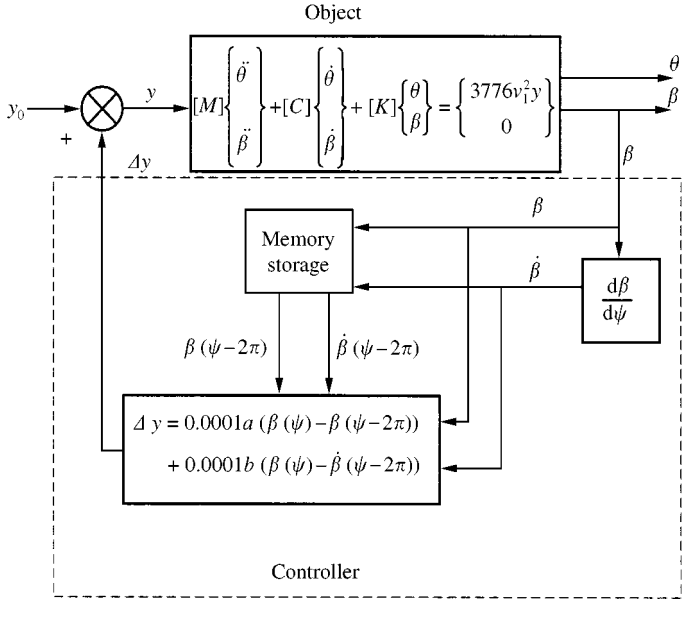

Figure 4. Schematic diagram of the control law applied to the helicopter rotor blade.

where

$$\mathbf{A} = \begin{bmatrix} 0 & 0{\cdot}3776 v_1^2 a \\ 0 & 0 \end{bmatrix}, \qquad \mathbf{B} = \begin{bmatrix} 0 & 0{\cdot}3776 v_1^2 b \\ 0 & 0 \end{bmatrix}. \tag{10}$$

In general, a particular solution $\mathbf{x}(\psi)$ of equation (9) for $\psi \geqslant 0$ is uniquely determined by the initial function $\mathbf{x}(\psi)$ which defines, for example, the position of the system for the time $-\tau \leqslant \psi \leqslant 0$.

The periodic particular solution of the controlled system (9) is identical to the periodic particular solution of the uncontrolled system (7).

4. PERTURBATION EQUATION FOR THE PERIODIC SOLUTION OF THE CONTROLLED SYSTEM

4.1. PERTURBATION EQUATION FOR HOVERING FLIGHT WITH ACTIVE CONTROL

For the case of hovering flight ($\mu = 0$), the equation of motion for the rotor blade with active control, according to equations (9) and (4), is

$$\mathbf{M} \cdot \ddot{\mathbf{x}} + \mathbf{C} \cdot \dot{\mathbf{x}} + \mathbf{K} \cdot \mathbf{x} = [3776 v_1^2 y_0, 0]^{\mathrm{T}} + \mathbf{A}(\mathbf{x}(\psi) - \mathbf{x}(\psi - \tau)) + \mathbf{B}(\dot{\mathbf{x}}(\psi) - \dot{\mathbf{x}}(\psi - \tau)), \tag{11}$$

where the matrices $\mathbf{M}$, $\mathbf{K}$ $\mathbf{C}$ and y_0 are time independent.

The particular solution of equation (11), which represents the steady state pitch and flap angles of the rotor blade in hovering flight, can be predicted as a vector of constant magnitudes $\mathbf{x}_0$ which according to equation (11) has the following form:

$$\mathbf{x}_0 = \mathbf{K}^{-1} \mathbf{y}_0. \tag{12}$$

Introduction of the perturbed motion

$$\mathbf{x}(\psi) = \mathbf{x}_0 + \Delta\mathbf{x}(\psi) \tag{13}$$

into the equation of motion (11), gives the perturbation equation

$$\mathbf{M} \cdot \Delta\ddot{\mathbf{x}} + \mathbf{C} \cdot \Delta\dot{\mathbf{x}} + \mathbf{K} \cdot \Delta\mathbf{x} = \mathbf{A}(\Delta\mathbf{x}(\psi) - \Delta\mathbf{x}(\psi - \tau)) + \mathbf{B}(\Delta\dot{\mathbf{x}}(\psi) - \Delta\dot{\mathbf{x}}(\psi - (\tau)). \tag{14}$$

4.2. PERTURBATION EQUATION FOR FORWARD FLIGHT WITH ACTIVE CONTROL

The equation of motion for the rotor blade in forward flight ($\mu > 0$) with active control is given by equation (9). In this case, the input from the pilot to the rotor $\mathbf{y}(\psi)$ is periodic with period $\tau = 2\pi$. The time delay used in the control terms is also equal to the period $\tau = 2\pi$. Therefore, the steady state solution for the system with control is periodic with period τ, and is identical to the steady state solution for the system without control,

$$\mathbf{x}_0(\psi) = \mathbf{x}_0(\psi + \tau). \tag{15}$$

Introduction of the perturbed motion

$$\mathbf{x}(\psi) = \mathbf{x}_0(\psi) + \Delta\mathbf{x}(\psi) \tag{16}$$

into the equation of motion (9) gives the perturbation equation about the steady state motion of the rotor blade in forward flight

$$\mathbf{M}(\psi)\cdot\Delta\ddot{\mathbf{x}} + \mathbf{C}(\psi)\cdot\Delta\dot{\mathbf{x}} + \mathbf{K}(\psi)\cdot\Delta\mathbf{x} = \mathbf{A}(\Delta\mathbf{x}(\psi) - \Delta\mathbf{x}(\psi-\tau)) + \mathbf{B}(\Delta\dot{\mathbf{x}}(\psi) - \Delta\dot{\mathbf{x}}(\psi-\tau)). \tag{17}$$

5. STABILITY ANALYSIS FOR HOVERING FLIGHT

5.1. STATE-SPACE FORMULATION AND THE CHARACTERISTIC EQUATION

The perturbation equation (14) can be written in terms of the state-space co-ordinates as follows:

$$\Delta\dot{\mathbf{Z}} = \mathbf{E}\cdot\Delta\mathbf{Z} + \mathbf{N}\cdot\Delta\mathbf{B}, \tag{18}$$

where

$$\mathbf{E} = \begin{bmatrix} 0 & \mathbf{I} \\ -\mathbf{M}^{-1}\mathbf{K} & -\mathbf{M}^{-1}\mathbf{C} \end{bmatrix}, \quad \mathbf{N} = \begin{bmatrix} \mathbf{0} & \mathbf{0} \\ \mathbf{0} & 0{\cdot}377v_1^2\mathbf{M}^{-1} \end{bmatrix}, \quad \Delta\mathbf{Z} = [\Delta\theta, \Delta\beta, \Delta\dot{\theta}, \Delta\dot{\beta}]^{\mathrm{T}},$$

$$\Delta\mathbf{B} = [0, 0, a(\Delta\beta(\psi) - \Delta\beta(\psi-\tau)) + b(\Delta\dot{\beta}(\psi) - \Delta\dot{\beta}(\psi-\tau)), 0]^{\mathrm{T}}. \tag{19}$$

The solution of equation (18) can be assumed to have the following form:

$$\Delta\mathbf{Z} = \Delta\mathbf{Z}_0\, \mathrm{e}^{\lambda\psi}. \tag{20}$$

Substitution of equation (20) into equation (18) results in a set of homogeneous algebraic equations that are linear with respect to the vector of constant magnitudes $\Delta\mathbf{Z}_0$. Therefore, the function (20) is the particular solution of equation (18) for the magnitudes λ which are roots of its characteristic equation:

$$\Delta = det[\mathbf{E} + \mathbf{N}\cdot\mathbf{W} - \lambda\mathbf{1}] = 0, \quad \mathbf{W} = \begin{bmatrix} 0 & 0 & 0 & 0 \\ 0 & 0 & 0 & 0 \\ 0 & a(1-e^{-2\pi\lambda}) & 0 & b(1-\mathrm{e}^{-2\pi\lambda}) \\ 0 & 0 & 0 & 0 \end{bmatrix}. \tag{21}$$

However, in contrast with the characteristic equation of the perturbation equation for the rotor blade without control, which has four characteristic roots, this characteristic equation (21) is transcendental and therefore has an infinite number of characteristic roots (see reference [5]). This is a consequence of the presence of the time-delay terms in the control law. To find the characteristic roots, the real and imaginary parts of the characteristic equation (21) were separated to produce two equations. The loci of zero points of the real and imaginary parts of the characteristic equation were plotted in the complex plane U–R. The characteristic roots are identified as the points in the complex plane where the loci intersect. The root of the characteristic equation, which has the largest real part, is called the "dominant" characteristic root. An example of a plot of the loci of zero points of the real and imaginary parts of the characteristic equation (21) is shown in Figure 5.

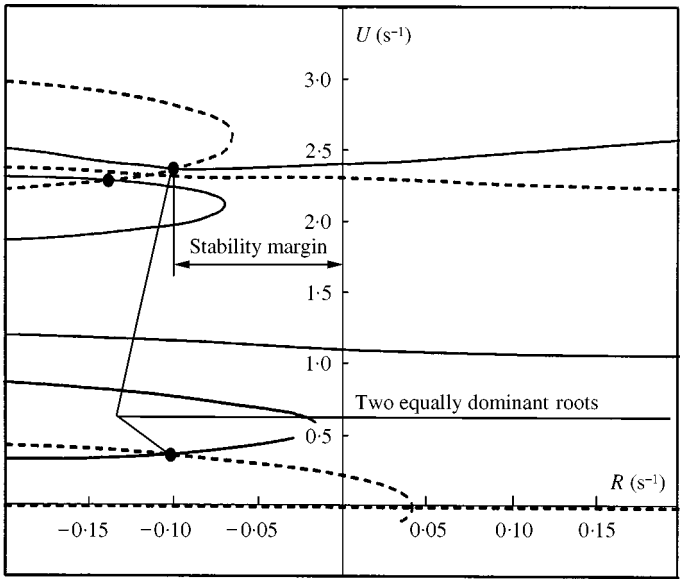

Figure 5. Roots of the characteristic equation for $\sigma = 0{\cdot}08$, $v1^2 = 10{\cdot}8$ and $a = 6{\cdot}75$ and $b = 0{\cdot}6$ s. ——, locus of zero points of the real part of the characteristic equation; ---- locus of zero points of the imaginary part of the characteristic equation, ● roots of the characteristic equation.

5.2. OPTIMAL VALUES OF THE CONTROL PARAMETERS

The optimal values of the control parameters a and b for specified values of the pitch natural frequency v_1 and centre of gravity offset σ, are the values that result in the lowest value of the real part of the dominant characteristic root R_{dom}. These values produce the largest increase in the stability margin of the steady state motion of the rotor blade. The global search for the optimal values of the control parameters was performed by a specially developed computer program. The minimum of the real part of the dominant root was considered as the goal function. For each point (a, b) of the search domain $a - b$, the computer program sought the dominant root as described in section 5.1. An example of results of the search is presented in Figure 6 for the design parameters $\sigma = 0{\cdot}08$ and $v_1^2 = 10{\cdot}8$.

5.3. RESULTS OF NUMERICAL COMPUTATION

The optimal values of the control parameters, and the corresponding lowest values of R_{dom}, have been found for a range of values of the pitch natural frequency v_1 and the centre of gravity offset σ. Figure 7 shows the increase in the region of asymptotical stability in the domain $\sigma - v_1^2$ results from the application of the control law.

A solid line shows the stability boundary for the controlled system and a broken line shows the stability boundary for the uncontrolled system. In the region labelled "unstable" the value of R_{dom} is positive; in the region labelled "stable" the value of R_{dom} is negative. In a significant part of the region (between the solid and broken lines in Figure 7) where the steady state motion is unstable without control, the control law is able to stabilize it.

In Figure 7, point P indicates the design parameters for which the contour plot of the real part of the dominant root is provided in Figure 6. It can be seen from Figure 6 that the uncontrolled system ($a = 0$ and $b = 0$) for the design parameters specified by the point P is

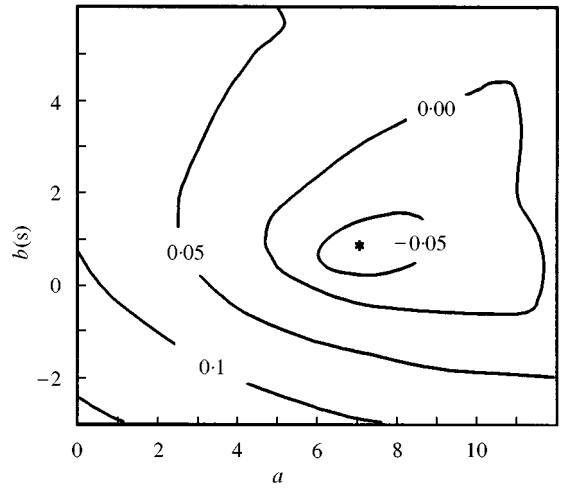

Figure 6. R_{dom} as function of a and b: $\sigma = 0{\cdot}08$, $v_1^2 = 10{\cdot}8$; * denotes optimal value of a and b.

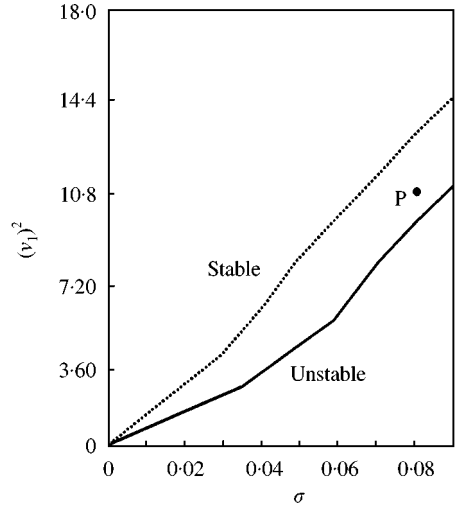

Figure 7. Stability boundaries in hovering flight with and without control; - - -, stability boundary without control; ——, stability boundary with control.

unstable ($R_{dom} = 0{\cdot}108\ s^{-1}$). For the optimal parameters ($a = 6{\cdot}75$ and $b = 0{\cdot}6$ s) the real part of the dominant root is negative ($R_{dom} = -0{\cdot}097\ s^{-1}$). It was observed that for the optimal parameters a and b two equally dominant roots of the same real part always exist. This peculiarity for the design parameters corresponding to the point P can be seen from Figure 5.

The developed method of searching for the optimal values of the control parameters a and b has been verified by numerical integration of the perturbation equation (14) using the Runge–Kutta method. The initial functions adopted for this integration were $\Delta\theta(\psi) = 0{\cdot}0$, $\Delta\beta(\psi) = 0{\cdot}1$, for $-2\pi \leqslant \psi \leqslant 0$. The results are shown in Figure 8.

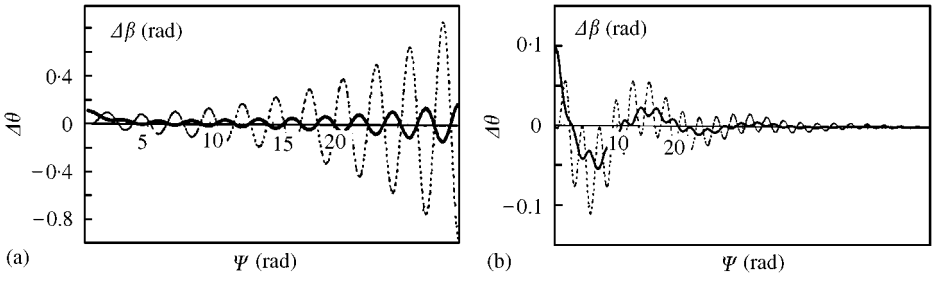

Figure 8. Perturbations of the uncontrolled and controlled system respectively; - - -, $\Delta\theta$ (rad); ———, $\Delta\beta$ (rad).

As expected, the amplitude of the perturbations for the uncontrolled system increases with time because the steady state motion is unstable, and the amplitude of the perturbations for the controlled system with the optimal values of the control parameters decreases with time because of steady state motion has been stabilized. Figure 8(b) shows clearly that for the optimal values of a and b, the oscillation of the rotor blade about the steady state motion is the superposition of frequencies corresponding to the imaginary parts of the two equally dominant roots shown in Figure 5.

6. STABILITY ANALYSIS FOR FORWARD FLIGHT

For the case of forward flight ($\mu > 0$), the perturbation equation (17) has periodic coefficients and time-delay terms. Since for an equation of this type a method to search for the dominant characteristic root is not yet developed, equation (17) was numerically integrated to investigate the stability of the periodic steady state motion of the rotor blade in forward flight.

The initial functions for the numerical integration of the perturbation equation (17) for all the cases studied were $\Delta\theta(\psi) = 0{\cdot}0$, $\Delta\beta(\psi) = 0{\cdot}1$ for $-2\pi \leqslant \psi \leqslant 0$. The value of the square of non-dimensional pitch natural frequency was $\nu_1^2 = 14{\cdot}4$. The figures described below illustrate a sample of the numerical analysis.

6.1. INFLUENCE OF FORWARD FLIGHT ON ROTOR BLADE STABILITY

The results in Figure 9 were calculated for the rotor blade without control ($a = b = 0$) and for a centre of gravity offset of $\sigma = 0{\cdot}064$. Figure 9(a) shows that for the case of hovering flight ($\mu = 0$) the amplitude of the perturbations increases with time, indicating that the steady state motion of the rotor blade is unstable; whereas Figure 9(b) shows that for the case of forward flight ($\mu = 0{\cdot}3$) the amplitude of the perturbations decreases with time, indicating that the periodic steady state motion of the rotor blade is stable. These two figures show that forward flight has a stabilizing effect on the motion of the rotor blade. Stammers [14] also found that the pitch-flap flutter stability margin of a helicopter rotor blade was greater in forward flight than in hovering flight.

6.2. INFLUENCE OF THE CENTRE OF GRAVITY OFFSET ON ROTOR BLADE STABILITY

Figure 10(a) shows the results for the rotor blade without control ($a = b = 0$) for the same forward flight condition ($\mu = 0{\cdot}3$) as the results in Figure 9(b), except that the value of the

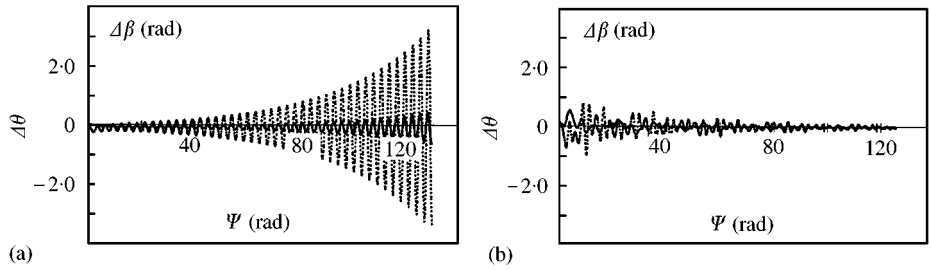

Figure 9. Perturbations about the steady-state motion of the rotor blade: (a) for the helicopter in hovering flight: $\mu = 0{\cdot}0$, $\sigma = 0{\cdot}064$, $a = b = 0$; (b) for the helicopter in forward flight: $\mu = 0{\cdot}3$, $\sigma = 0{\cdot}064$, $a = b = 0$. ——, $\Delta\beta$, - - -, $\Delta\theta$.

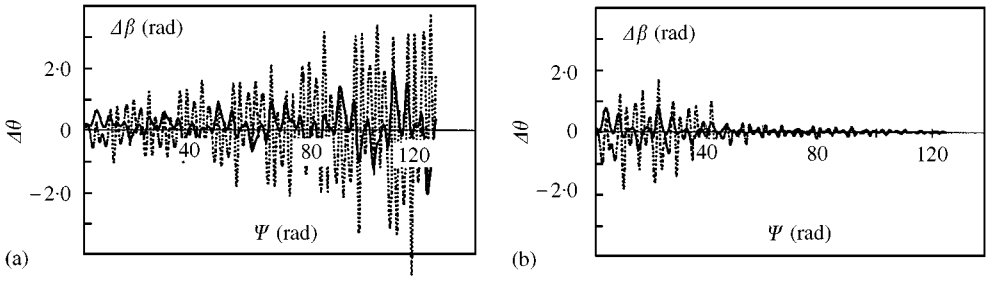

Figure 10. Perturbations about the steady state motion of the rotor blade: (a) for the helicopter in forward flight without control: $\mu = 0{\cdot}3$, $\sigma = 0{\cdot}069$, $a = b = 0$; (b) for the helicopter in forward flight with control, $\mu = 0{\cdot}3$, $\sigma = 0{\cdot}069$, $a = 7{\cdot}0$, $b = -5{\cdot}0$ s. ——, $\Delta\beta$, - - -, $\Delta\theta$.

centre of gravity offset has been increased from $\sigma = 0{\cdot}064$ to $0{\cdot}069$, which represents moving the centre of gravity slightly towards the trailing edge of the rotor blade. Figure 10(a) shows that this increase in the value of σ causes the periodic steady state motion of the rotor blade to become unstable and the perturbations to grow with time. Therefore, for $v_1^2 = 14{\cdot}4$ the stability boundary lies between $\sigma = 0{\cdot}064$ and $0{\cdot}069$.

6.3. INFLUENCE OF THE CONTROL LAW ON ROTOR BLADE STABILITY

The results in Figure 10(b) have been calculated for the same forward flight condition ($\mu = 0{\cdot}3$) as those in Figure 10(a). However, the control law has been introduced to the mathematical model of the system by setting $a = 7{\cdot}0$ and $b = -5{\cdot}0$ s. These values of the control parameters were found by the largest gradient method of optimization. The equations of perturbations (17) were numerically integrated for the assumed control parameters a and b and the same initial functions $\Delta\theta(\psi) = 0{\cdot}0$, $\Delta\beta(\psi) = 0{\cdot}1$, for $-2\pi \geqslant \psi \leqslant 0$. The goal function was defined as a minimum of the time necessary for the system response along co-ordinates $\Delta\theta(\psi)$ and $\Delta\beta(\psi)$ to be smaller than $0{\cdot}1$. Figure 10(b) shows that the application of the control law with these values of the control parameters causes the periodic steady state motion of the rotor blade that was unstable without control to become stable. This demonstrates the effectiveness of the control law in stabilizing the periodic motion of the rotor blade in forward flight.

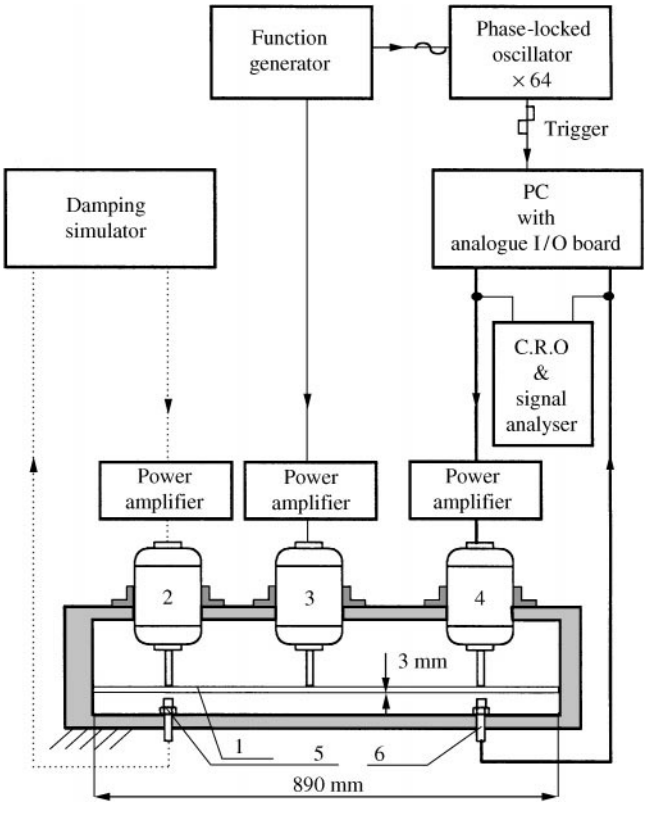

Figure 11. Schematic diagram of the laboratory installation; 1—flexible beam, 2, 3, 4 — electro–magnetic exciters, 5, 6 — eddy current displacement transducers.

7. EXPERIMENTAL INVESTIGATION

7.1. DESCRIPTION OF THE LABORATORY INSTALLATION

The aims of the experimental investigation were to test the effectiveness of the control law on a real mechanical system, and to determine whether the optimal values of the control parameters can be found experimentally with no knowledge of the dynamic properties of the system. As would be the case for a real helicopter, the laboratory installation in this experimental investigation is treated as a "black box" whose steady state motion is periodic. The controller must be able to sense this period and adjust the time delay in the control law to be equal to this period.

The mechanical part of the laboratory installation consists of a steel bar 1, rigidly supported at each end, with three electromechanical exciters 2, 3, 4 attached to it. The first two natural frequencies of the system were 24 and 59 Hz.

The middle exciter 3 provided a steady sinusoidal excitation to the steel bar to induce the periodic motion of the installation. It was driven by a *function generator* via a *power amplifier* as shown in Figure 11.

The exciter 2 provided a force that was proportional to the velocity of the steel bar. The displacement of the steel bar at the location of the left-hand exciter 2 was sensed by

a displacement transducer and then electronically differentiated by the *damping simulator* to produce a signal proportional to the velocity. This was used to apply a negative damping force in order to make the motion of the system unstable.

The exciter 4 in Figure 11 provided the control force. The time delay in the feedback path was synchronized with the period of the excitation force applied to the system by the middle exciter. This was achieved by using a *phase-locked oscillator*. The input to the *oscillator* was the same sine wave from the function generator that was used to drive the power amplifier for the exciter 3. The *oscillator* produced a square wave with a frequency 64 times that of the sine wave. The square wave from the oscillator was used to trigger the analogue/digital (A/D) converter on the *I/O board* connected to the *PC*. For each trigger, the position of the system was recorded in a *circular buffer* with the help of the right-hand displacement transducer 6. Using the data stored in this circular buffer an *interrupt service routine* performed the following operations: numerical differentiation of the displacement to obtain the velocity; reading from memory the displacement and velocity recorded 64 samples earlier; calculation of the control signal according to the control law (1); and sending the control signal to the D/A converter for conversion to an analogue signal to drive the exciter 4 via the *power amplifier*.

Between triggers the PC had to complete the interrupt service routine. The oscillator constructed for these experiment was accurate up to a maximum excitation frequency of 50 Hz. With that input frequency, the frequency of the output square wave from the oscillator was 3200 Hz. With the A/D converter being triggered at a frequency of 3200 Hz, the PC was easily able to complete the interrupt service routine before the next trigger came. By comparison, the Sikorsky Black Hawk helicopter rotor rotates at 258 rpm, which is only 4.3 Hz. Thus, in terms of computer processing power, it would be easy to implement the control law on a helicopter.

7.2. PROCEDURE FOR THE EXPERIMENTAL DETERMINATION OF THE STABILITY MARGIN

In order to determine the improvement of the stability margin of the periodic motion of the laboratory installation due to the control law (1), the following procedure was used.

For the selected excitation frequency f_{ex} and the control parameters a and b, the gain of the power amplifier of the exciter 3 was adjusted to produce periodic response of the system of amplitude 0·075 mm as measured by the transducer 5. Then the amount of negative damping c added to the controlled object was increased up to the magnitude that caused instability. The maximal amount of negative damping which could be added to the controlled system before the periodic motion became unstable c_{max} was used to measure the increase in stability margin achieved by applying the control law (1). The amount of negative damping which could be added to the uncontrolled object ($a = b = 0$) before the periodic motion became unstable c_{ref} was used as a reference. The percentage increase in c_{max} relative to c_{ref} was computed according to

$$\Delta c = 100 \times (c_{max} - c_{ref})/c_{ref}. \tag{22}$$

The records of the motion of the laboratory installation comprise time-series plots and frequency spectrum plots (see Figure 12).

Each of the time-series plots shows two traces. The upper trace is the displacement of the bar d in mm as measured by the right-hand displacement transducer 6. The lower trace shows the control signal Δy in V measured at the output of the D/A converter, which was produced by the real-time control program running on the PC.

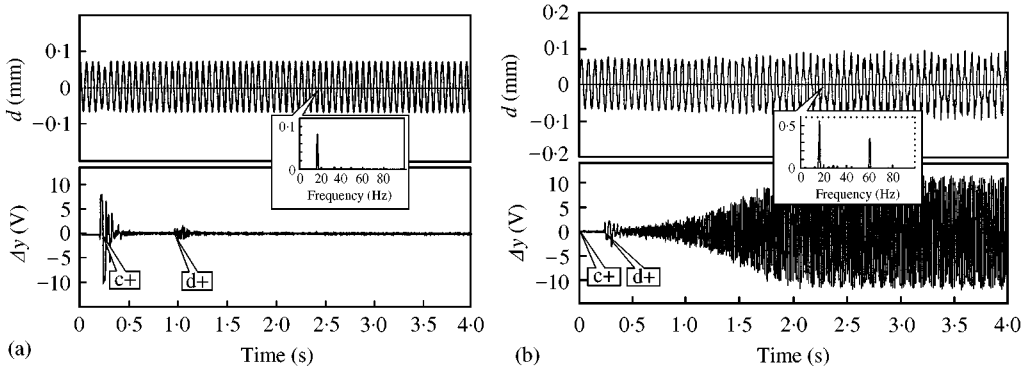

Figure 12. Examples of periodic motion of the laboratory installation; $f_{ex} = 16$ Hz, $a = -0{\cdot}1$, $b = -0{\cdot}2$ s: (a) stable; (b) unstable.

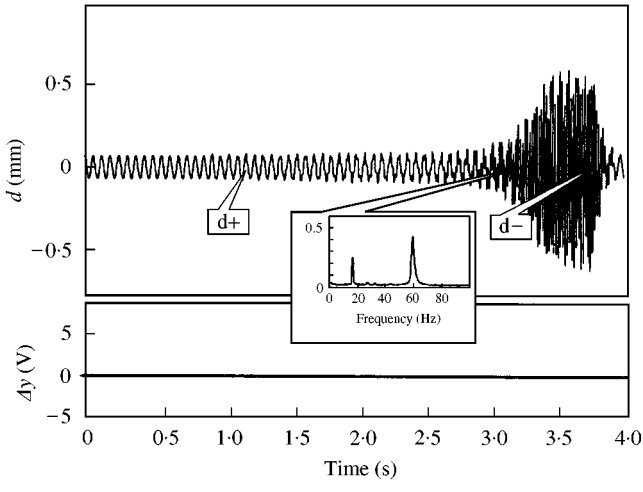

Figure 13. An example of the unstable periodic motion of the laboratory installation: $f_{ex} = 16$ Hz, $a = 0$, $b = 0$ s.

The marks c+, c−, d+ and d− correspond to those instants of time when: the control signal was applied to the system, the control signal was removed, the negative damping was applied to the object and the negative damping was removed. The periodic motion of the system is described as having become unstable either: when the amplitude of the control signal grew until it was "saturated", that is, until it reaches the limits of the D/A converter which was $\pm$ 10 V; or when the amplitude of the oscillations of the steel bar grew beyond the admissible range $\pm$ 0·5 mm.

The time-series plot in Figure 12(a) began at $t = 0$ s with no control and no negative damping added to the system. At $t = 0{\cdot}2$ s (c+) the control was added to the system. A large transient oscillation in the control signal can be seen at this point, but it quickly died away and the control signal settled down to a very small amplitude. This transient occurred because all the values in the memory locations of the "circular buffer" were set to zero when the real-time control program was started. At $t = 1.0$ s (d+) the negative damping was added to the system. A small transient in the control signal occurred at this point but it quickly settled

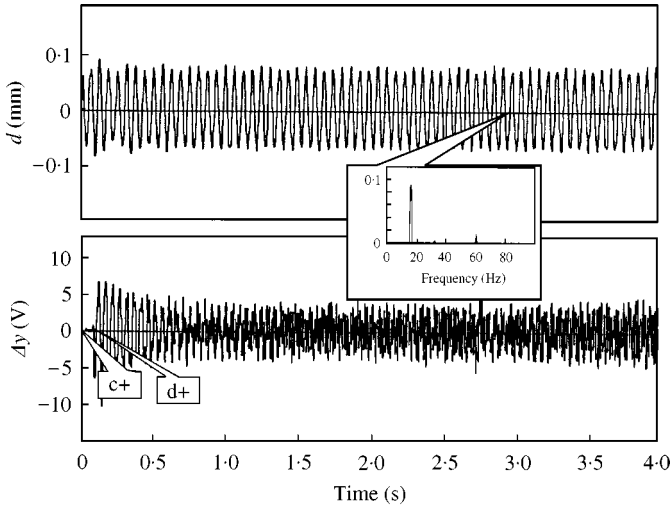

Figure 14. An example of the periodic motion of the laboratory installation being at the boundary of stability; $f_{ex} = 16$ Hz, $a = 0{\cdot}35$, $b = -0{\cdot}15$ s.

back to a small amplitude. The frequency spectrum plot corresponding to $t = 2{\cdot}0$ s shows that the only significant component of the oscillation is at the excitation frequency of 16 Hz. Such a recorded periodic motion was considered stable. In this case, the amount of negative damping added to the system was increased to a magnitude c_1 less than the value of c_{max}.

The time-series plot in Figure 12(b) presents the case when the amount of negative damping added to the system was increased to a magnitude c_2 greater than the value of c_{max}. At $t = 0$ s the control had been added to the system. The negative damping was added at $t = 0{\cdot}3$ s and the control signal grew to saturation. Motion of the system was no longer periodic at 16 Hz but had an additional significant component at 60 Hz. Such a periodic motion of the laboratory installation was considered unstable. Therefore, the maximum negative damping is $c_1 < c_{max} < c_2$.

Figure 13 presents the case when the amount of negative damping that was added to the system without control ($a = b = 0$) made the periodic motion unstable. The negative damping was added at $t = 1{\cdot}2$ s and had to be removed at $t = 3{\cdot}7$ s because the oscillation became too violent. The corresponding frequency spectrum plot shows the perturbations at a frequency of 59 Hz which grew very large. Such a periodic motion of the laboratory installation was considered unstable.

Figure 14 presents the case when the response of the control system is not periodic but both the control signal and the response of the system are well within the admissible ranges. The frequency spectrum plot shows the presence of small disturbances of frequency 59 Hz. In such cases, the periodic motion of the system is considered to be on the boundary of stability and the corresponding magnitude of the negative damping was considered to be maximal.

7.3. EXPERIMENTAL DETERMINATION OF THE OPTIMAL VALUES OF THE CONTROL PARAMETERS

In the experiments, the frequency of the sinusoidal excitation f_{ex} provided by the function generator was varied over a wide range. At each excitation frequency, the values of the

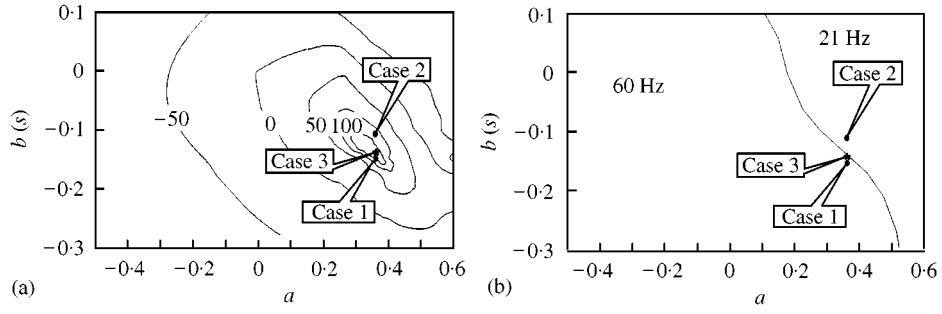

Figure 15. (a) Margin of stability Δc as a function of the control parameters a and b. (b) Frequencies of perturbations f_u as a function of the control parameters; $f_{ex} = 16$ Hz.

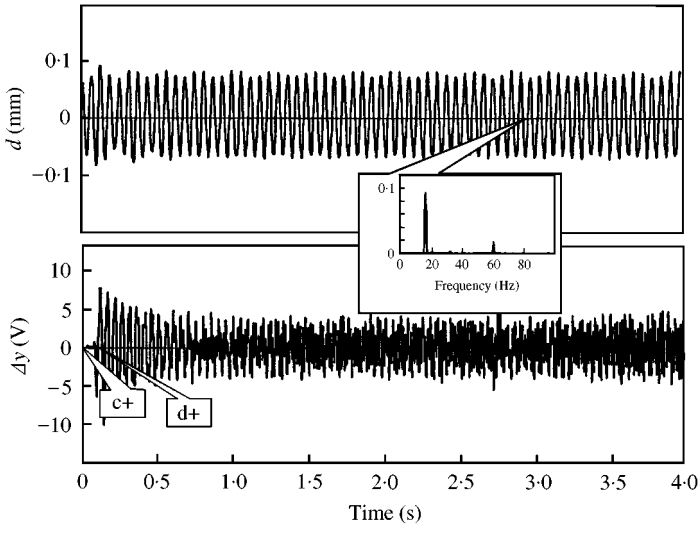

Figure 16. The time-series and spectrum plot for case 1.

control parameters a and b in the control law (1) were varied in a trial-and-error fashion in order to find the most effective values for stabilizing the periodic motion of the system. The values of a and b which gave the highest value of Δc were considered to be the optimal ones. The contour plot of Δc as a function of a and b for the excitation frequency of 16 Hz is shown in Figure 15(a). Figure 15(b) shows frequencies of perturbations f_u over the same region of the control parameters a and b.

To illustrate the significant features of the contour plots of Δc and f_u shown in Figure 15, let us consider three cases of the recorded motion marked by dots in Figure 15. All cases have the same value of $a = 0{\cdot}35$. The optimal value of $\Delta c = 200\%$ was found to occur in this region and is marked by an asterisk in Figure 15.

For $a = 0{\cdot}35$, there are two distinct frequency regions in the contour plot of f_u as a function of a and b in Figure 15 (b). For $b = -0{\cdot}15$ s, the frequency of the perturbations was 60 Hz; and for $b = -0{\cdot}11$ s the frequency of the perturbations was 21 Hz. The point where the optimal values of a and b occur ($a = 0{\cdot}35$, $b = -0{\cdot}14$ s) lies on the border between the 21 and 60 Hz regions.

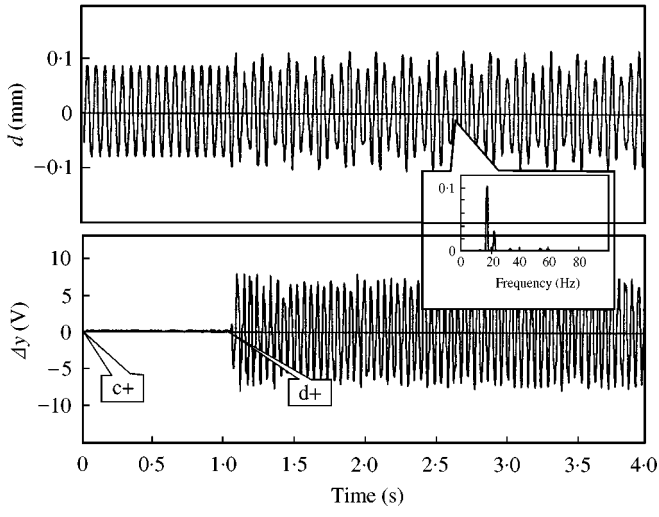

Figure 17. The time-series and spectrum plot for case 2.

Case 1: $a = 0{\cdot}35$, $b = -0{\cdot}15$ s: This case shows that for the values of the control parameters $a = 0{\cdot}35$, $b = -0{\cdot}15$ s the frequency of the perturbations f_u was 60 Hz. The value of Δc for this case was significantly less than the maximum value. This can be seen from the closely spaced contour lines in this region in Figure 15(a).

The time-series plot in Figure 16 illustrates a situation where the periodic motion is at the boundary of stability. In this situation the controller was not able to suppress the perturbations completely, and the amplitude of the control signal in the steady state was significantly greater than zero. When the negative damping was added, a large transient oscillation occurred in the control signal. Over the next 0·8 s the amplitude of the control signal decreased, but it then remained constant at 8 V peak to peak, which was 40% of its saturated value. The displacement trace shown in Figure 16 is clearly not pure 16 Hz oscillation. From the corresponding spectrum plot, it is easy to see that the perturbations have frequency equal to 60 Hz.

Case 2: $a = 0{\cdot}35$, $b = -0{\cdot}11$ s: The time-series plot in Figure 17 shows that the control became almost saturated when negative damping was added to the controlled system at $t = 1{\cdot}0$ s. However, very marked difference can be seen between the frequency of the oscillation of the control signal in this plot and that in Figure 16. The perturbations, as it can be seen from the spectrum plot, have a frequency of 21 Hz. In this case, a small change in the value of b from $-0{\cdot}15$ to $-0{\cdot}11$ s caused the value of f_u to change from 60 to 21 Hz.

Case 3: $a = 0{\cdot}35$, $b = -0{\cdot}14$ s: The values of the control parameters used in this case were the optimal values where the greatest value of Δc was found to occur for $f_{ex} = 16$ Hz. This can be seen in Figure 15(a) where the point $a = 0{\cdot}35$, $b = -0{\cdot}14$ s lies in the $\Delta c = 150$–200% region of the contour plot.

The time-series plot in Figure 18 shows that the periodic motion became unstable after the negative damping was increased to a value greater than c_{max}. For 1 s after this increase, the high-frequency component of the control signal grew slowly. Over the next 0·5 s the amplitude of the control signal grew more rapidly unit it became saturated. At this point, $t = 1{\cdot}8$ s, the amplitude of the displacement had not increased significantly but a higher frequency component can be seen to be present. The frequency spectrum plot corresponding to the displacement at $t = 1{\cdot}8$ s reveals two significant components of frequency at about 21

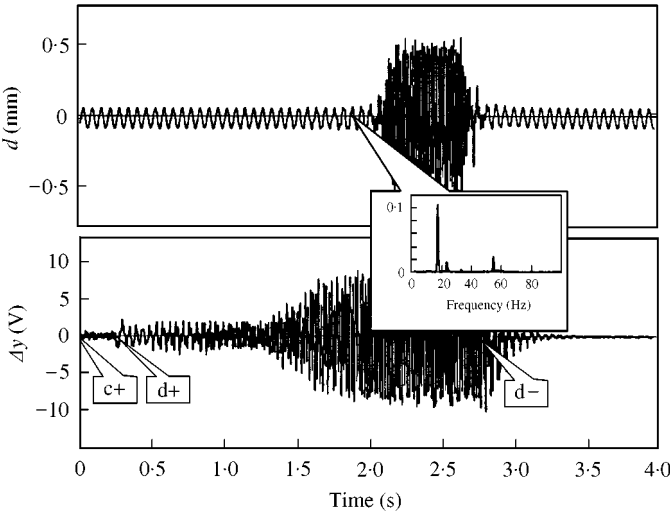

Figure 18. The time-series and spectrum plot for case 3: $a = 0{\cdot}35$, $b = -0{\cdot}14$ s.

and 59 Hz in addition to the 16 Hz component. This confirms the results shown for $a = 0{\cdot}35$, $b = -0{\cdot}14$ s in Figure 15(b) where the optimal values of a and b lie on the borderline between two significantly different values of f_u.

This phenomenon was also detected by means of the numerical investigations described earlier. The optimal values of the control parameters a and b occur where two roots have the same value of the real part and are thus equally dominant. The imaginary parts of these two roots are not the same, and so they correspond to different frequencies of perturbations about the periodic steady state motion. Adjusting the control parameters away from this optimal point will cause one of the roots to move to the right in the complex plane and the other to move to the left. Which of the two roots moves to the right and which moves to the left depends on how the values of the control parameters are changed.

7.4. MARGIN OF STABILITY AS A FUNCTION OF EXCITATION FREQUENCY

To evaluate the effectiveness of the control law (1), the highest achievable value of Δc was determined for a wide range of excitation frequencies of the periodic motion. The optimal values of Δc and the corresponding optimal values of a and b are plotted as a function of the period of the harmonic excitation force (T_{ex}) in Figure 19.

This plot shows that the effectiveness of the control law depends on the period of the harmonic excitation T_{ex}. For the controlled system with the optimal values of the control parameters, the margin of stability Δc is greater than zero for all periods of excitation T_{ex}.

For the range of values of T_{ex} used in the experimental results shown in Figure 19, the values of T_{ex} for which the control law (1) was least effective was the period corresponding to the second natural frequency of the uncontrolled system ($T_2 = 0{\cdot}017$ s) and integer multiples of this period. As can be seen from Figure 11, the exciter 2, simulating the negative damping, was installed in the middle between nodes of the second mode. Therefore, the instability of the second mode was promoted in the laboratory installation. The results presented in Figure 19 show a similar pattern to those found numerically for the mathematical model of a one-d.o.f. system considered in references [6, 7]. It was found that

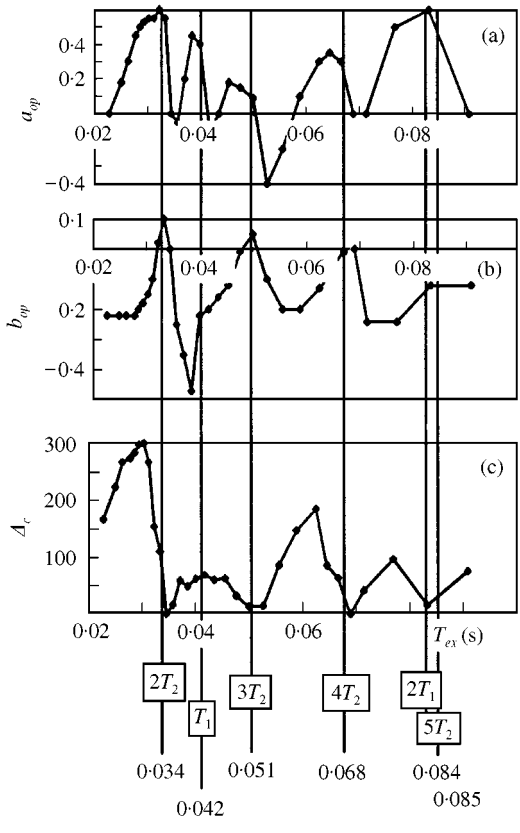

Figure 19. (a) Optimal magnitudes of the control parameter a. (b) Optimal magnitudes of the control parameter b. (c) Margin of stability Δc.

the periods of the harmonic excitation for which the control law (1) was least effective were the period corresponding to the natural frequency of the system and integer multiples of that period.

8. CONCLUSIONS

A new control law for stabilizing the periodic motion of uncertain systems has been tested using a two-d.o.f. mathematical model of a helicopter rotor blade, including the aerodynamic forces. A method has been developed to search the complex plane for the dominant characteristic root of the perturbation equation and to find the optimal values of the control parameters.

The controlled system with the optimal values of the control parameters was found to have two equally dominant characteristic roots. The corresponding oscillation is a combination of two distinct frequencies.

The developed control law stabilizes the periodic steady state motion of the uncontrolled system without changing it. The control law improves the stability of the steady state motion of a helicopter rotor blade in both hovering flight and forward flight. It has been shown that in both cases a significant improvement of the stability margin can be achieved

by applying the control law with the optimal values of the control parameters. The control law significantly increases the region of asymptotic stability of the rotor blade in the domain $\sigma - v_1^2$.

If the mathematical model is not available, the optimal values of the control parameters would have to be determined experimentally. The experiments using a simple laboratory installation have demonstrated that the optimal values of the control parameters can be determined in this way.

It has been demonstrated that the optimal values of the control parameters can be found experimentally with no knowledge of the dynamics of the system or the equations of motion. The effectiveness of the control law has been determined experimentally as a function of the period of the motion being stabilized. The values of T_{ex} for which the control law (1) is least effective are the periods corresponding to natural frequencies of the uncontrolled system and integer multiples of these periods.

The second term introduced in equation (1) plays a very significant role in improving the stability of the steady state motion of the system. Figures 6 and 15(a) illustrate this fact. It can be seen that the optimal performance is not achieved when the control parameter b is equal to zero. By adjusting it to the optimal value one can significantly improve the stability margin of the periodic motion of the system considered.

REFERENCES

1. R. G. Loewy 1984 *Journal of the American Helicopter Society* **29**, 4–30, Helicopter vibrations: a technological perspective.
2. W. G. Bousman and W. R. Mantay 1987 *Proceedings of the NASA/Army Rotorcraft Technology Conference, Ames Research Centre, Moffett Field*, CA 17–19 March, *NASA* CP-2495, 180–311. A review of research in rotor loads.
3. R. A. Ormiston, W. G. Warmbrodt, D. H. Hodges and D. A. Peters 1987. *Proceedings of the NASA/Army Rotorcraft Technology Conference, Ames Research Centre, Moffett Field, CA, NASA CP*-2495, 353–529. Rotorcraft aeroelastic stability.
4. C. C. Crawford 1990 *Journal of The American Helicopter Society* **35**, Rotorcraft analytical improvement needed to reduce development risk.
5. J. M. Krodkiewski and J. S. Faragher 1995 *Proceedings of the International Conference on Vibration and Noise*, Venice, Vol. 1, 766–774. Stability improvement of the periodic motion of non-linear systems.
6. J. S. Faragher 1996 *Ph.D. thesis, University of Melbourne*. Stability improvement of periodic motion of helicopter rotor blades.
7. Pyragas 1992 *Physics Letters A* **170**, 421–428. Continuous control of chaos by self-controlling feedback.
8. J. Shaw, N. Albion, E. J. Hanker and R. S. Teal 1989 *Journal of the American Helicopter Society* **31**, 14–25. Higher harmonic control: wind tunnel demonstration of fully effective vibratory hub force suppression.
9. W. R. Splettstoesser, R. Kube, W. Wagner, U. Seelhorst, A. Boutier, F. Micheli, E. Mercker and K. Pengel 1997 *Journal of the American Helicopter Society* **42**, 58–78. Key results from higher harmonic control aeroacoustic rotor test (HART).
10. N. D. HAM 1987 *Vertica* **11**, 109–122. Helicopter individual blade control research at MIT 1977–1985.
11. S. Jacklin, A. Blaas, D. Teves and R. Kube 1995 51*st Annual Forum Proceedings — American Helicopter Society*, Vol. 1, 662–680. Reduction of helicopter BVI noise, vibration, and power consumption through individual blade control.
12. Chopra 1996, *SPIE Proceedings*, Vol. 2717, *The International Society for Optical Engineering*, WA, DC. Smart structures and materials 1996: smart structures and integrated systems.
13. P. P. Friedmann and T. Z. Millott 1995 *Journal of Guidance, Control and Dynamics* **18**, 664–673. Vibration reduction in rotorcraft using active control: a comparison of various approaches.
14. C. W. Stammers 1970 *Aeronautical Quarterly* 18–48. The flutter of a helicopter rotor blade in forward flight.